Highly efficient orange–red electroluminescence from a single layer MEH-PPV-POSS:CdS0.75Se0.25 hybrid PLED

Materials Science and Engineering B 177 (2012) 921–928

Contents lists available at SciVerse ScienceDirect

Materials Science and Engineering B

journal homepage: www.elsevier.com/locate/mseb

Highly efficient orange–red electroluminescence from a single layer MEH-PPV-POSS:$CdS_{0.75}Se_{0.25}$ hybrid PLED

Gamze Saygili[a,b], Gülçin Ünal[c], Serdar Özçelik[c], Canan Varlikli[a,*]

[a] Ege University, Solar Energy Institute, 35100 Bornova-Izmir, Turkey
[b] Vestel Electronic, MOS, 45030 Manisa, Turkey
[c] Department of Chemistry, İzmir Institute of Technology, 35430 Urla-İzmir, Turkey

ARTICLE INFO

Article history:
Received 26 December 2011
Received in revised form 18 March 2012
Accepted 16 April 2012
Available online 28 April 2012

Keywords:
Organic light emitting diodes
Conjugated polymer
Hybrid systems
Quantum dots
Nanocomposites

ABSTRACT

In this study, poly[2-methoxy-5-(2-ethylhexyloxy)-1,4-phenylenevinylene] end capped with polyhedral oligomeric silsesquioxanes (MEH-PPV-POSS): cadmium sulfide selenide quantum dots ($CdS_{0.75}Se_{0.25}$ QDs) nanocomposites based OLEDs were fabricated. By the addition of $CdS_{0.75}Se_{0.25}$ QDs into the polymer active layer, a considerable enhancement was observed in terms of hole and electron injection in devices. Additionally, the presence of QDs reduced the interchain interaction of polymer that resulted in narrower electroluminescence (EL) spectrum. The device structure of ITO/PEDOT: PSS/MEH-PPV-POSS: 25 wt% $CdS_{0.75}Se_{0.25}$/Ca (40 nm)/Al demonstrated the best performance with a brightness of 8672 cd/m^2 at 10 V, current efficiency of 2.5 cd/A at 8 V, and an EQE of 0.55% at 150 mA/cm^2.

1. Introduction

Organic light emitting diodes (OLEDs) represent one of the optoelectronic devices that have a great potential on replacement of current technologies in both display and lighting application fields. The use of conjugated polymers as active organic materials in these devices provide many advantages such as simple processing, color variety, low turn-on voltage, light weight, large area, flexibility and low cost [1–5]. However, they still have some fundamental limitations such as, imbalance of hole and electron fluxes due to high electron injection barrier and low electron mobility and formation of aggregates and/or excimers due to the interchain interaction in most of organics. Among the strategies used to overcome these limitations, the addition of quantum dots (QDs) into the polymer matrix would be an attractive approach since the polymer/QD composites have presented highly enhanced optical and electrical properties.

Several groups have reported successful combinations of II–IV semiconductor nanoparticles, such as cadmium selenide (CdSe), cadmium sulfide (CdS) core QDs or cadmium selenide/zinc sulfide (CdSe/ZnS) core/shell QDs with polymers, such as a polymer derivative of 9,9-dioctylfluorene and 2,1,3-benzothiadiazole (PFBT8) or poly[2-methoxy-5-(2-ethylhexyloxy)-1,4-phenylenevinylene] (MEH-PPV). The improved results by incorporation of conventional binary QDs are summarized in Table 1 [6–11]. In such hybrid system, where electroluminescence originates only from the polymer, QDs enhance a particular property of polymer (not overall optical behavior) by their superior charge carrier mobility and stability. It is also reported that QDs neutralize the defects in the polymer matrix resulting in an enhanced structural stability of polymer [8]. They may act as hole trapping centers that serve to a better balance of charge carriers and cause a decrease in the interchain interaction of the polymer [10].

In general, optical properties of binary QDs can be tuned by controlling their size and composition. In case of the alloyed QDs (i.e. CdSSe) optical properties are tailored not only by size dependent quantum confinement effect but also by controlling composition of the components of alloyed materials [12]. In this study, the precursor of sulfur and selenium along with cadmium are used to obtain colloidal alloy of cadmium sulfide selenide ($CdS_{0.75}Se_{0.25}$) capped with trioctylphosphine oxide (TOPO) as an organic ligand and used as a dopant in a MEH-PPV-POSS based OLED. The advantage of the ternary alloyed QDs are to produce improved optical and electrical properties as well as enhanced device performances due to fine tuning of composition of QDs at a constant size [13]. Nonetheless, to the best of our knowledge, no study to date in literature has reported the incorporation of $CdS_{0.75}Se_{0.25}$ and highly efficient hybrid OLED

* Corresponding author. Tel.: +90 232 3111244; fax: +90 232 3886027.
E-mail address: canan.varlikli@ege.edu.tr (C. Varlikli).

0921-5107/$ – see front matter © 2012 Elsevier B.V. All rights reserved.
http://dx.doi.org/10.1016/j.mseb.2012.04.011

Table 1
The reported efficiencies in the literature for MEH-PPV: QD composite based PLEDs in which the electroluminescence has been obtained from polymer.

Ref. #	Device structure	Brightness [cd/m^2] (V_{appl})	Current efficiency [cd/A] (V_{appl})	EQE [%]	Power efficiency [lm/W]	Operating voltage [V]	FWHM [nm]	$\lambda_{EL\,max}$ [nm]	Active area (mm^2)
[6]	ITO/MEHPPV/Al	6 (9 V)	–	–	–	6	–	590	–
	ITO/MEHPPV: aggregated 10 wt% CdSe/Al	60 (8 V)	–	–	–	5	–	590	–
[7]	ITO/PEDOT: PSS/PFBT8/LiF/Al	–	–	1	–	10	–	~530	–
	ITO/PEDOT: PSS/PFBT8: 5 wt% CdSe/LiF/Al	–	–	>1	–	4	–	~530	–
[8]	ITO/PEDOT: PSS/MEHPPV/Al	~25 (12 V)	<0.005			8		590	4
	ITO/PEDOT: PSS/MEHPPV: 0.4 wt% CdSe (ZnS)/Al	~100 (12 V)	~0.02			7	–	590	4
[9]	ITO/PEDOT: PSS/FP-PPV-co-MEH-PPV/Ca/Al	3949 (10 V)	0.27 (10 V)	–	–	4	–	560	4
	ITO/PEDOT: PSS/FP-PPV-co-MEH-PPV: CdSe (ZnS)/Ca/Al	8192 (7 V)	1.27 (7 V)	–	–	4	–	560	4
[10]	ITO/PEDOT: PSS/MEH-PPV-POSS/Ca/Al	1083 (10 V)	0.63 (8 V)	–	0.14	2.2	87	588	12
	ITO/PEDOT: PSS/MEH-PPV-POSS: 0.3 wt% $CuInS_2$/Ca/Al	2701 (10 V)	0.89 (8 V)	–	0.20	2.1	73	588	12
[11]	ITO/PEDOT: PSS/MEH-PPV/Al	12 (75 mA/cm^2)	–	–	–	13	–	590	–
	ITO/PEDOT: PSS/MEH-PPV: 20 wt% CdSe (ZnS)/Al	290 (75 mA/cm^2)	–	–	–	21	–	> 590	–

devices based on MEH-PPV-POSS: $CdS_{0.75}Se_{0.25}$ nanocomposites (Table 2).

2. Experimental

2.1. Preparation of Se precursor (NaHSe)

Sodium borohydrate ($NaBH_4$, Riedel de Haen) and selenium powder (Aldrich) were mixed in a flask at room temperature and kept under nitrogen atmosphere for a few minutes. And 6 ml of ultra pure water was added into the flask and the solution was refluxed for 1 h to obtain transparent NaHSe solution [14]. According to the reaction presented below, $NaBH_4$ leads to the reduction of selenium.

$$4NaBH_{4(aq)} + 2Se_{(s)} \rightarrow 2NaHSe_{(aq)} + Na_2B_4O_{7(s)} + 14H_{2(g)}$$

Fresh NaHSe solution was used without any purification for each experiment since it can be oxidized easily when exposed to air.

2.2. Synthesis and characterization of ternary alloyed quantum dots

Ternary-alloyed colloidal nanocrystals were synthesized in one step and one-pot based on the two – phase method introduced by Pan et al. for core/shell QDs [15]. In their synthetic pathway, the colloidal CdSe nanocrystals was first prepared and purified, and then in the second-step, thiourea and cadmium myristate were added to the purified CdSe solution to form core–shell CdSe/CdS nanocrystal [15]. We modified the method to synthesize alloyed QDs. The modification applied is the mixing of aqueous solution of NaHSe and thiourea with non-aqueous solution of cadmium myristate and TOPO in one-pot and one-step, forming the ternary-alloyed nanocrystals. The synthesis was briefly described here and the details will be published elsewhere. Cadmium oxide (Alfa Aesar) and myristic acid (Sigma Aldrich) were reacted at 250 °C for 2 h to form cadmium myristate. Cadmium myristate (0.4 g) and 2 g of TOPO were dissolved in toluene (80 ml), and kept at 80 °C. NaHSe (3 mg) and thiourea (60 mg) were dissolved in nitrogen-saturated water (80 ml) and heated to 100 °C for 30 min. Cadmium myristate and surfactant dissolved in toluene at 80 °C was transferred to aqueous solution of NaHSe and thiourea while stirring it. The

Table 2
Performances of hybrid PLEDs with the device structure of ITO/PEDOT: PSS/MEH-PPV-POSS: *x* wt% $CdS_{0.75}Se_{0.25}$/Ca/Al at 1000 cd/m^2.

Dopant amount [*x* wt%]	Voltage [V]	Current density [mA/cm^2]	Current efficiency [cd/A]	EQE [%]	Power efficiency [lm/W]	$\lambda_{EL\,max}$ [nm] at 6 V	FWHM [nm]
0	6.7	96	1.00	0.23	0.43	588	87
5	6.7	92	1.06	0.23	0.49	588	87
10	6.0	85	1.21	0.27	0.63	588	84
15	5.4	72	1.28	0.28	0.75	588	82
25	4.7	67	1.42	0.43	0.92	588	81
50	4.9	204	0.47	0.11	0.30	588	75

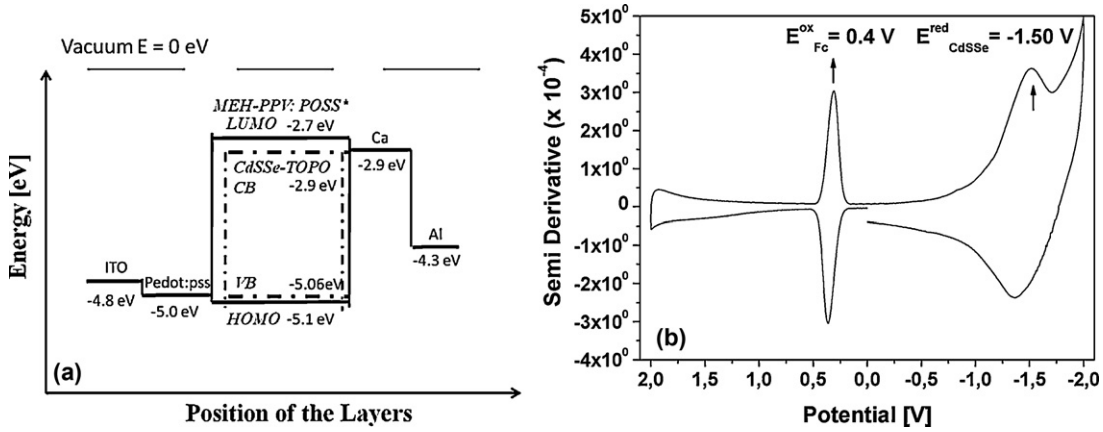

Fig. 1. (a) Energy level diagram for MEH-PPV-POSS: $CdS_{0.75}Se_{0.25}$ composite based hybrid PLED and (b) semi derivative of cyclic voltammogram of $CdS_{0.75}Se_{0.25}$ versus Fc. *HOMO and LUMO energy levels of MEH-PPV-POSS were taken from the literature [18]

co-existence of precursors of Se and S ensures the formation of the alloyed nanocrystals. The colloidal alloys began to form within 30 min. Aliquots were taken from the reaction flask to monitor the formation of the alloy by UV–vis absorption and fluorescence (Varian Cary 5 and Eclips spectrophotometers) and dynamic light scattering (DLS) measurements.

The alloyed nanocrystals were purified by precipitation with ethyl alcohol and redispersed in toluene. The purification step was applied several times to remove excess capping agent and impurities. The purified nanocrystals were kept dry at room temperature.

It is important to note that optical and structural properties of the alloys are strongly dependent on the mole ratio of precursors, reactivity of precursors, reaction time, temperature, volume of the reaction, etc. A comprehensive study tuning the photophysical properties of the alloyed nanocrystals controlling size and composition will be published elsewhere.

In order to calculate the fluorescence quantum yield (Φ_f) of the alloyed nanocrystals, Rhodamine 6G was used as reference ($\Phi_f = 0.9$ in ethanol [16]). The crystal structure and the mole ratio of the precursors (chemical composition) of the nanocrystals were characterized by Phillips X'Pert Pro diffractometer equipped with Cu Kα radiation. The XRD data for indexing was recorded in step-scanning mode in the angular range $10 < 2\theta < 65^\circ$. EDX analysis was conducted to support the composition of the alloyed nanocrystals. The hydrodynamic size and size distribution were determined by DLS method. Size analysis of the nanocrystals

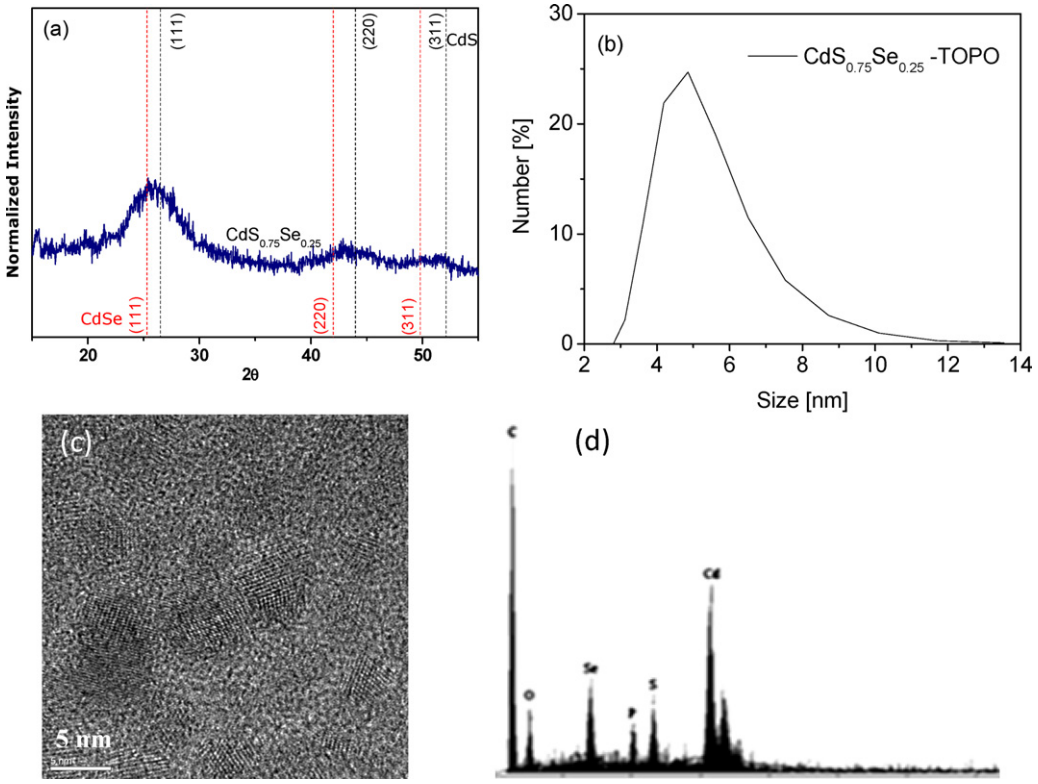

Fig. 2. (a) Powder XRD pattern, (b) particle size distribution, (c) HRTEM image and (d) EDX result of TOPO capped $CdS_{0.75}Se_{0.25}$ QDs. The composition is determined by XRD and EDX analysis. EDX analysis also proves the existence of TOPO. The diffraction lines of the alloyed nanocrystal $CdS_{0.75}Se_{0.25}$ falls between the lines defined for the pure CdS and CdSe.

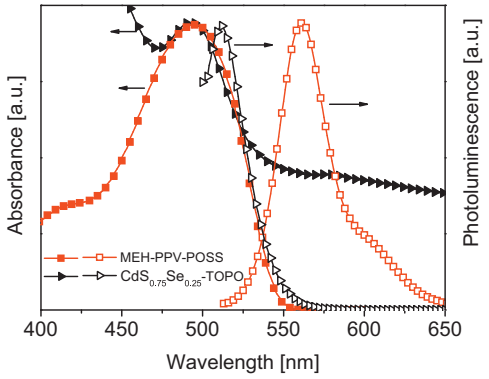

Fig. 3. The normalized absorption and PL spectra of pure MEH-PPV-POSS and $CdS_{0.75}Se_{0.25}$ QDs in chlorobenzene.

dispersed in toluene was performed by a Malvern Nanosizer NS.

Conduction band (CB) energy level of the nanocrystals was determined as −2.9 eV by using CH Instrument 660 B potentiostat. Platin wire and 0.1 M $TBAPF_6$ in acetonitrile were used as counter electrode and electrolyte, respectively. The nanocrystals coated on TCO working electrode exhibited reduction potential at −1.5 V versus Ag/AgCl reference electrode where inner reference Ferrocene/Ferrocenium couple showed oxidation potential at 0.4 V. The optical band gap (E_{OBG}) was calculated from the absorption spectrum edge of the nanocrystals as 2.14 eV. The valance band (VB) energy level of the nanocrystals was estimated from CB and E_{OBG} [17]. HOMO and LUMO energy levels of MEH-PPV-POSS were taken from the literature [18]. The energy level diagram of the composite device and cyclic voltammogram of $CdS_{0.75}Se_{0.25}$ QDs versus Ferrocene (Fc) are shown in Fig. 1.

2.3. Optical studies of blends and device fabrication

MEH-PPV-POSS polymer was provided by American Dye Source Comp. and used without any further purification. For the PL studies in solution phase, $CdS_{0.75}Se_{0.25}$ QDs and MEH-PPV-POSS solutions were prepared in chlorobenzene separately. By adding 1 μl of MEH-PPV-POSS solution (V_{total}; 8 μl, 2.5×10^{-6} M) into the $CdS_{0.75}Se_{0.25}$ solution, the changes in PL intensity of $CdS_{0.75}Se_{0.25}$ were monitored. In order to investigate the effect of $CdS_{0.75}Se_{0.25}$ on PL characteristics of the polymer in film phase, MEH-PPV-POSS/$CdS_{0.75}Se_{0.25}$ composites with the content of 0, 5, 10, 15, 25, 50 wt% $CdS_{0.75}Se_{0.25}$ were spin coated at 2500 rpm on glass slides and their thin film PL measurements were performed. Absorption and PL spectra were obtained by Analytik Jena S600 UV–Vis and PTI-QM1 luminescence spectrophotometers, respectively. The fluorescence quenching rate constant (kq, $M^{-1}\,s^{-1}$) was calculated by the Stern–Volmer equation [19].

For the device fabrication, indium thin oxide (ITO) coated glass substrate (Delta Comp., 10 Ω/□) was cleaned with routine chemical method then treated with O_2 plasma under the conditions of, 10^{-2} mbar, 60 W and 2 min. A ~40 nm thick of poly(ethylenedioxythiophene): poly(styrenesulfonate) (PEDOT: PSS) with the conductivity of 1 S/cm (Sigma–Aldrich) was coated as a hole transport material (HTM) at 4000 rpm onto pre-cleaned ITO substrate and dried at 120 °C for 0.5 h under vacuum. MEH-PPV-POSS polymer and $CdS_{0.75}Se_{0.25}$ solutions (10 mg/ml) were dissolved in chlorobenzene separately. They were mixed at different ratios (0, 5, 10, 15, 25 and 50 wt% of $CdS_{0.75}Se_{0.25}$). Thereafter, ~90 nm thick films were spin coated at 2500 rpm on to the PEDOT: PSS layer and dried at 80 °C for 1 h in vacuum. Finally, 40 nm thick Ca and 100 nm thick Al electrodes were deposited with using a shadow mask by vacuum thermal evaporation technique (VTE) at 10^{-6} mbar.

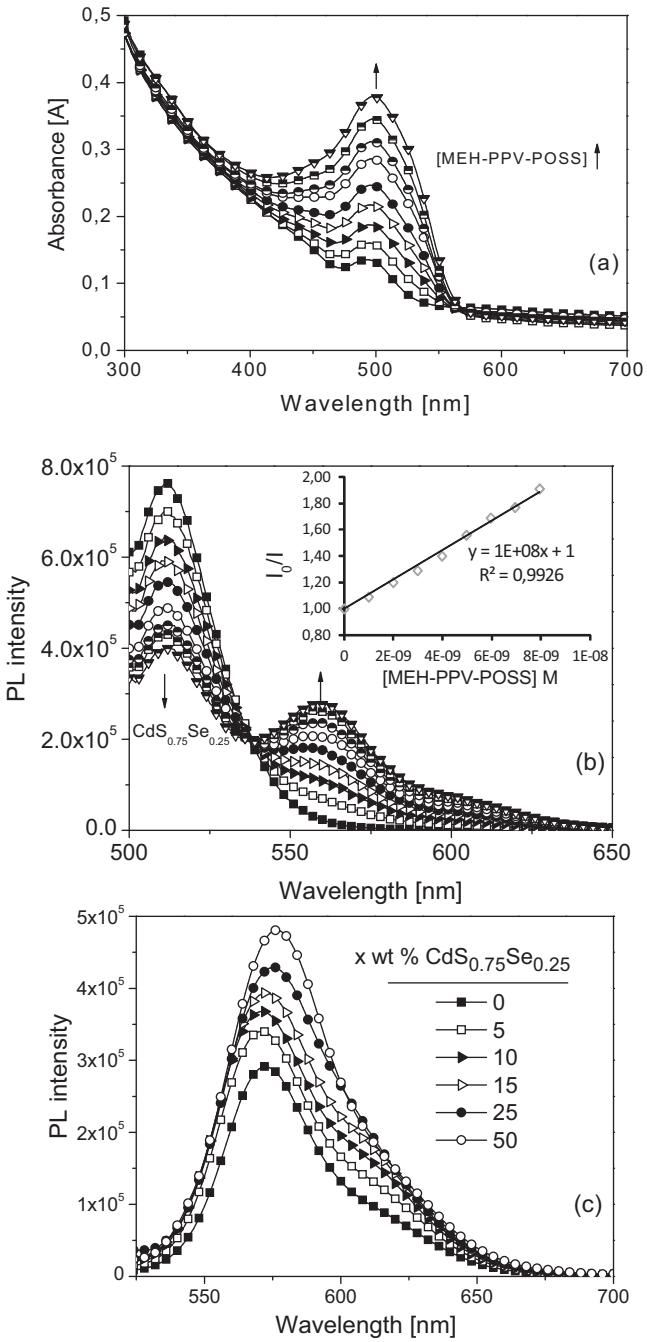

Fig. 4. (a) The absorption spectra, (b) quenching of PL intensity of $CdS_{0.75}Se_{0.25}$ QDs by the addition of MEH-PPV-POSS in chlorobenzene (λ_{exc} = 495 nm), the relevant Stern-Volmer plot (inset), and (c) PL spectra of thin films of MEH-PPV-POSS: $CdS_{0.75}Se_{0.25}$ composites.

The polymer film thicknesses were measured by using Ambios XP-1 high-resolution surface profiler, while the thickness of cathode was observed via a quartz crystal monitor. To determine the contribution of $CdS_{0.75}Se_{0.25}$ QDs on electrical mechanism of MEH-PPV-POSS based device, hole-only and electron-only devices were fabricated with the structures of ITO/PEDOT: PSS/MEH-PPV-POSS: x wt% $CdS_{0.75}Se_{0.25}$/Au and Al/PEDOT: PSS/MEH-PPV-POSS: x wt% $CdS_{0.75}Se_{0.25}$/Ca/Al, respectively. Keithley 2400 Source-Unit was used for electrical characterizations. The electroluminescence measurements were carried out by using Ocean Optics USB-4000

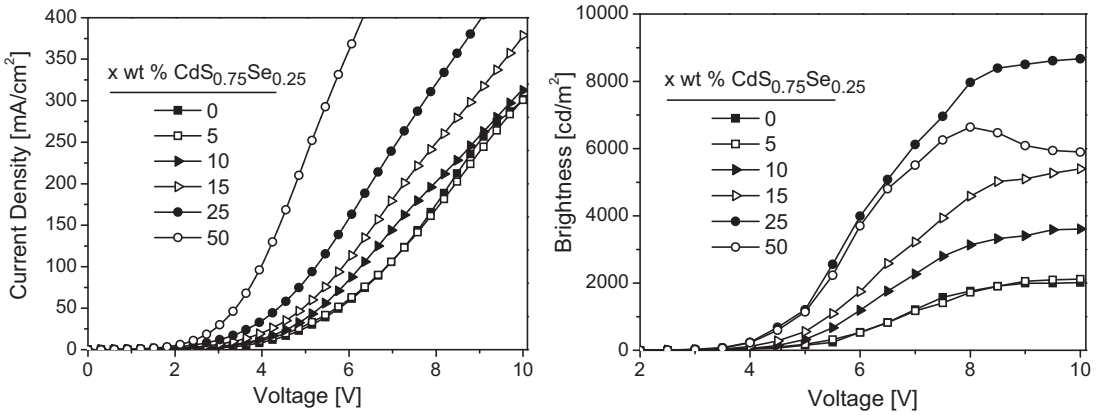

Fig. 5. Current density and brightness versus voltage characteristics of the MEH-PPV-POSS: $CdS_{0.75}Se_{0.25}$ composites based PLEDs.

Spectrophotometer. The active area was 12 mm^2 and five parallel devices were performed for each device. All device characterizations were performed under inert conditions.

Transmission electron microscopy (TEM) observation was carried out using a Tecnai G^2 F30, operating at 100 kV. For TEM experiments, the samples were spin-coated onto Si-wafer as thin films with 90 nm thickness. Focused ion beam (FIB) sample preparation was performed using a FEI Nova600i Nanolab Dual Beam SEM/FIB system. A standard ion column is installed, which allows Ga milling at 2–30 kV. The ion column axis was positioned under an angle of 52° in respect to the electron column axis. The system was also equipped with an in situ gas injection system loaded with a Pt deposition needle and an OMNIPROBE TM extraction needle.

3. Results and discussion

3.1. Chemical composition and structural properties of alloyed $CdS_{0.75}Se_{0.25}$ QDs

The reactivity and the initial amount of sulfur and selenium precursors are important parameters to tune the chemical composition and as a result the optical properties of the alloyed QDs. The chemical composition of the CdS_xSe_{1-x} alloy was determined by using the Vegard's law [20]. Fig. 2(a) showed XRD pattern of green emitting, TOPO capped alloyed nanocrystals. By comparing hkl indices of bulk CdS and CdSe, the crystal structure of alloyed nanocrystals was verified to be face centered cubic. The chemical composition, particularly the percent ratio of sulfur and selenium in the alloy, was resolved by using the XRD pattern given in Fig. 2(a). We ascertained the composition of the alloyed nanocrystal used in this work *as* $CdS_{0.75}Se_{0.25}$. Fig. 2(c) is a HRTEM image of the nanocrystals, exhibiting size, the crystalline nature and the lattice planes of the QDs. The crystalline size of the QDs was found to be 5.0 nm by the use of XRD spectrum [21]. Furthermore, HRTEM based EDX analysis as given in Fig. 2(d) confirmed the chemical composition of the alloyed nanocrystals. The EDX analysis also provided existence of coating agent TOPO. The hydrodynamic size of the nanocrystals was measured by DLS (Fig. 2(b)). The hydrodynamic size of QDs was around 5.2 nm and the size distribution was monodispersed. The size estimated from XRD confirmed with the size measured by HRTEM and DLS. The chemical composition of the ternary-alloyed nanocrystals was unambiguously determined by XRD and EDX analyses.

3.2. Optical studies and device fabrication

Fig. 3 shows the optical properties of pure MEH-PPV-POSS polymer and $CdS_{0.75}Se_{0.25}$ QDs in chlorobenzene. The absorption peak of the pure MEH-PPV-POSS is located at 499 nm, which is attributed to π–π^* transitions and the maximum emission peak is located at 560 nm with an interchain emission peak at around 600 nm [22]. $CdS_{0.75}Se_{0.25}$ QDs exhibits maximum absorption intensity at 495 nm and an emission intensity at 512 nm with a Φ_f value of 0.80. The absorption spectra and quenching of PL intensity of $CdS_{0.75}Se_{0.25}$ QDs by the addition of MEH-PPV-POSS solution are shown in Fig. 4(a) and (b). Although it is not possible to distinguish the contributions of $CdS_{0.75}Se_{0.25}$ and MEH-PPV-POSS in absorption spectra of composite films, broadening of the spectrum and increase in the intensity can be attributed to the increase in MEH-PPV-POSS concentration. As the content of MEH-PPV-POSS

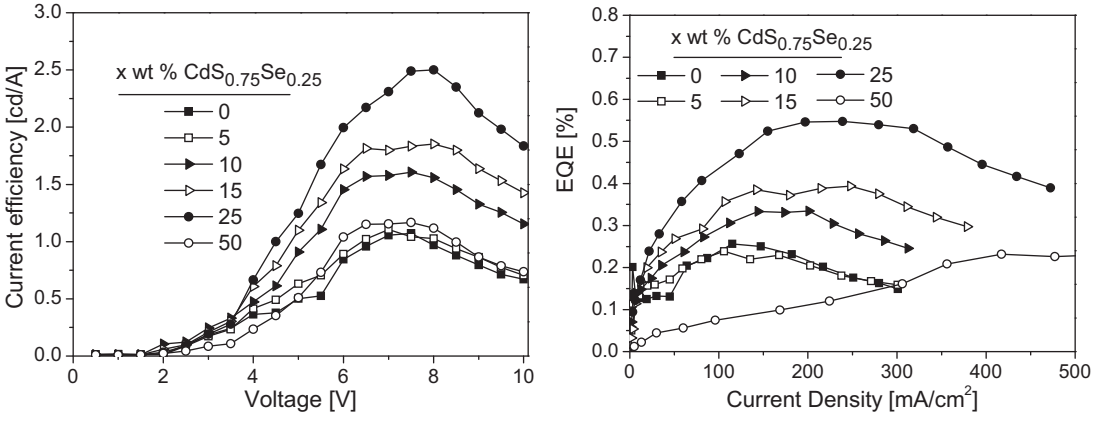

Fig. 6. Current efficiency-voltage and EQE versus current density characteristics of MEH-PPV-POSS: $CdS_{0.75}Se_{0.25}$ composites based PLEDs.

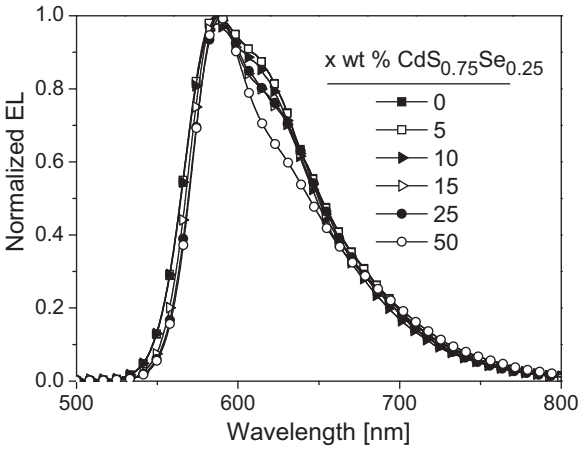

Fig. 7. Normalized EL spectra of devices based on MEH-PPV-POSS: $CdS_{0.75}Se_{0.25}$ composites and pure MEH-PPV-POSS under the applied voltage of 8 V.

increased in the composites, an increase in PL intensity of MEH-PPV-POSS was observed as expected. At the same time, the intensity of the $CdS_{0.75}Se_{0.25}$ emission was remarkably reduced resulting in a significant k_q value of $5 \times 10^{15}\ M^{-1}\ s^{-1}$. In Fig. 4(c), PL spectra of composite films are shown together with that of the pure polymer film for comparison. All spectra indicate that the emission originates from the polymer in the composite thin films. Moreover, a slight red shift and narrowing in the PL spectra with an enhanced intensity were observed depending on the increase in $CdS_{0.75}Se_{0.25}$ content. Since there is a big overlap between the absorption spectrum of MEH-PPV-POSS and the emission spectrum of $CdS_{0.75}Se_{0.25}$ QDs, the PL enhancement in film phase and high k_q value can be assigned to a possible energy transfer from QDs to the polymer.

3.3. Electrical and optical characterization of hybrid devices

Polymer: QD hybrid devices were fabricated with various concentration of $CdS_{0.75}Se_{0.25}$ QDs. Current density and luminance performance of these devices are shown in Fig. 5 as a function of voltage. The turn-on voltage was decreased from 2.3 V to 2 V and the current density was significantly increased as the concentration of $CdS_{0.75}Se_{0.25}$ QDs increases that indicate the presence of higher number of charge carriers in the composite based devices and a modification in the transport mechanism (Table 2). As can be seen from the energy band diagram in Fig. 1, $CdS_{0.75}Se_{0.25}$ QDs has larger electron affinity than that of the polymer. Due to the smaller electron injection barrier at the cathode/$CdS_{0.75}Se_{0.25}$ interface, more electrons are easily injected from the cathode to $CdS_{0.75}Se_{0.25}$ QDs and transferred to the polymer. This improved electron injection with the increased $CdS_{0.75}Se_{0.25}$ QD concentration leads to, not only an enhanced electrical characteristic, but also a significant enhancement in terms of brightness and electroluminescence (EL) intensity. The pure MEH-PPV-POSS based PLED exhibits a maximum brightness of 2015 cd/m^2 at 10 V, while the current efficiency and external quantum efficiency (EQE) were obtained 1.0 cd/A and 0.24% at 7 V (105 mA/cm^2), respectively (Fig. 6). By incorporation of 25 wt% $CdS_{0.75}Se_{0.25}$ QDs, the brightness was increased approximately 4.3-fold (8672 cd/m^2 at 10 V) and the device has a current efficiency of 2.3 cd/A and EQE of 0.48% at 7 V (240 mA/cm^2). Fig. 7 shows the normalized EL spectra of these devices. All spectra are similar in shape and position of main peak at 588 nm, accompanied by an interchain emission at around 615 nm. Additionally, the interchain emission was significantly reduced by incorporation of $CdS_{0.75}Se_{0.25}$ QDs into MEH-PPV-POSS polymer that results in a 12 nm decrease in the full width at half maximum (FWHM).

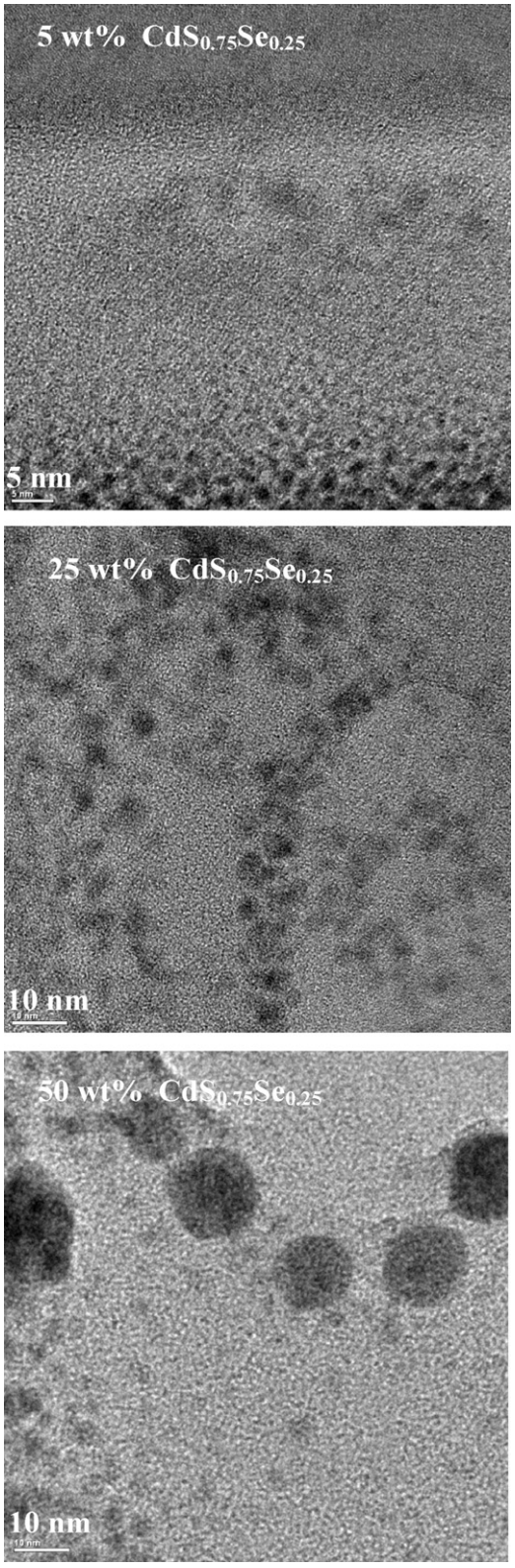

Fig. 8. TEM images of MEH-PPV-POSS: $CdS_{0.75}Se_{0.25}$ composite films including, (a) 5, (b) 25, and (c) 50 wt% of $CdS_{0.75}Se_{0.25}$.

It is clear that $CdS_{0.75}Se_{0.25}$ QDs reduced the interchain interaction as observed in PL spectra of the composite films because of its well-dispersed structuring in the polymer matrix. TEM images of MEH-PPV-POSS: $CdS_{0.75}Se_{0.25}$ composite films are shown in Fig. 8(a)–(c). $CdS_{0.75}Se_{0.25}$ nanoparticles are observed as dark gray

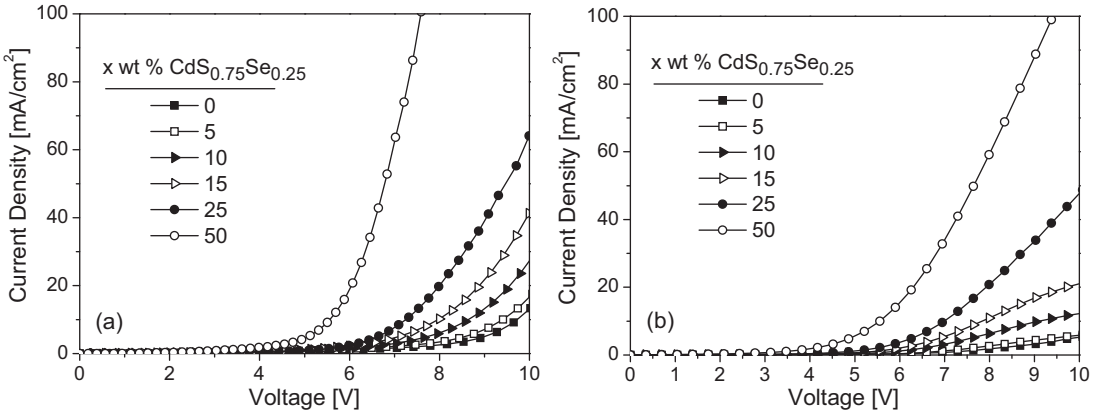

Fig. 9. The electrical characteristics of (a) hole-only [ITO/MEH-PPV-POSS: *x* wt% $CdS_{0.75}Se_{0.25}$/Au (50 nm)] and (b) electron-only [Al (65 nm)/MEH-PPV-POSS: *x* wt% $CdS_{0.75}Se_{0.25}$/Ca (40 nm)/Al (100 nm)] devices.

spots. For the 5 wt% of $CdS_{0.75}Se_{0.25}$ content, QDs could be observed in only some part of the polymer film. Therefore, its limited contribution on reduction of interchain emission and enhancement of electrical characteristics can be explained with the low concentration of $CdS_{0.75}Se_{0.25}$ (Fig. 8(a)). One of the factors to achieve the enhanced device performance can be assigned to the presence of homogeneously dispersed QDs, which were observed for the composite with the 25 wt% $CdS_{0.75}Se_{0.25}$ content (Fig. 8(b)). It is known that the dispersion of small size QDs into the polymer leads to the segregated polymer chain, reduced defects and enhanced structural stability of the polymer resulted in an enhanced electrical and optical device performance [10]. In the case of 50 wt% doping of $CdS_{0.75}Se_{0.25}$, the formation of $CdS_{0.75}Se_{0.25}$ globules over 10 nm were observed together with the well-dispersed small size $CdS_{0.75}Se_{0.25}$ QDs (Fig. 8(c)). It is assumed that these QD globules caused to a significant increase in current density for the device based on MEH-PPV-POSS: 50 wt% $CdS_{0.75}Se_{0.25}$ composite because of the increase of charge injection depending on $CdS_{0.75}Se_{0.25}$ concentration. However, degradation mechanisms of MEH-PPV and organics (small molecules, polymers) due to the high temperatures caused by high current density were reported by several groups [23,24]. As a result, the considerable drop in performance of the 50 wt% $CdS_{0.75}Se_{0.25}$ doped device can be explained by the effect of QD globules.

The current density–voltage characteristics of hole-only and electron-only devices based on MEH-PPV-POSS: $CdS_{0.75}Se_{0.25}$ composites are given in Fig. 9(a) and (b). Depending on increased concentration of $CdS_{0.75}Se_{0.25}$ QDs, both hole and electron current densities were significantly improved (Fig. 9(b)). It is clear that the $CdS_{0.75}Se_{0.25}$ QDs make a considerable contribution for the charge injection and transport resulting in an increase in the current density of the main devices. Fig. 10 shows the schematic mechanism for the MEH-PPV-POSS: $CdS_{0.75}Se_{0.25}$ composite based device that was similarly presented in a review [25]. It is assumed that the well-dispersed $CdS_{0.75}Se_{0.25}$ QDs modified the morphology of the polymer and led to larger contact surface at the both emissive layer/anode and emissive layer/cathode interfaces. Additionally, due to the higher electron affinity or lower CB and well-matched VB of $CdS_{0.75}Se_{0.25}$ QDs (Fig. 1), more electrons and holes are injected from relevant contacts, resulting in an increase in current density of electron-only, hole-only and also main devices.

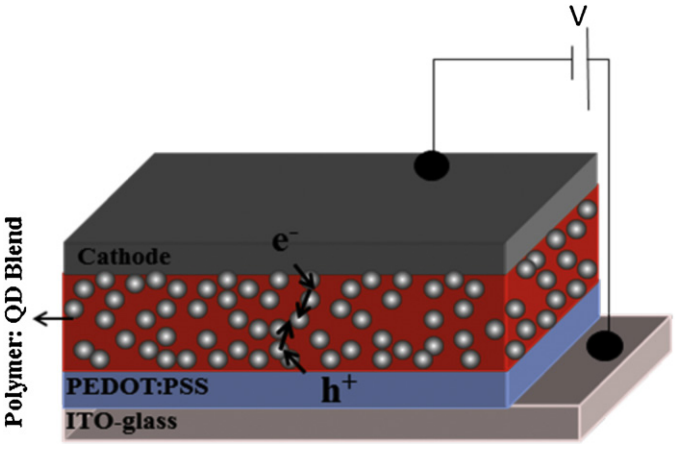

Fig. 10. The mechanism of improved charge carrier transport in a PLED based on MEH-PPV-POSS: $CdS_{0.75}Se_{0.25}$ composite as an active layer.

4. Conclusion

In summary, highly efficient single layer OLEDs were fabricated by using MEH-PPV-POSS: $CdS_{0.75}Se_{0.25}$ QDs nanocomposites as an active layer. It is assumed that well-dispersed structuring of $CdS_{0.75}Se_{0.25}$ QDs into the polymer matrix and well-matched CB and VB energy levels led to a reduced interchain interaction of polymer and a better injection of charge carriers from the relevant contacts. $CdS_{0.75}Se_{0.25}$ QDs may also improve the surface of polymer/cathode and polymer/anode by decreasing the direct interaction of polymer and contacts resulting in a reduced quencher points at the surface. The device structure of ITO/PEDOT: PSS/MEH-PPV-POSS: 25 wt% $CdS_{0.75}Se_{0.25}$/Ca (40 nm)/Al demonstrated the best performance with a brightness of 8672 cd/m^2 (10 V), current efficiency of 2.5 cd/A (8 V), and EQE of 0.55% (150 mA/cm^2), respectively.

Acknowledgements

We acknowledge the project support funds of Ege University (project contract #: 11GEE011), State Planning Organization of Turkey and The Scientific and Technological Research Council of Turkey (project contract #: 110T465). We thank Michael Brast from Device Technology of RWTH Aachen University for his supports.

References

[1] R.H. Friend, R.W. Gymer, A.B. Holmes, J.H. Burroughes, R.N. Marks, C. Taliani, D.D.C. Bradley, D.A. Dos Santos, J.L. Brédas, M. Lögdlund, W.R. Salaneck, Nature 397 (1999) 121–128.
[2] Y. Cao, I.D. Parker, G. Yu, C. Zhang, A.J. Heeger, Nature 397 (1999) 414.
[3] M.T. Bernius, M. Inbasekaran, J. O'Brien, W. Wu, Advanced Materials 12 (2000) 1737–1750.

[4] J.H. Park, K.J. Lee, O.O. Park, J.W. Yu, Y.C. Kim, J.K. Kim, Chemical Physics Letters 386 (2004) 101–104.
[5] H.Y. Low, S.J. Chua, Materials Letters 53 (2002) 227–232.
[6] J.H. Park, S.I. Park, T.H. Kim, O.O. Park, Thin Solid Films 515 (2007) 3085–3089.
[7] D. Zhu, H. Ye, H. Zhen, X. Liu, Synthetic Metals 158 (2008) 879–882.
[8] C.W. Lee, C. Renaud, C.S. Hsu, T.P. Nguyen, Nanotechnology 19 (2008) 455202, 7 pp.
[9] C.W. Lee, C.H. Chou, J.H. Huang, C.S. Hsu, T.P. Nguyen, Materials Science and Engineering B 147 (2008) 307–311.
[10] G. Saygili, C. Ozsoy, I. Oner, C. Zafer, C. Varlikli, S. Icli, Synthetic Metals 161 (2011) 196–202.
[11] S. Madan, J. Kumar, D. Madhwal, I. Singh, P.K. Bhatnagar, P.C. Mathur, Journal of Nanophotonics 5 (2011) 053518.
[12] M.D. Regulacio, M.Y. Han, Accounts of Chemical Research 43 (2010) 621–630.
[13] W. Ma, et al., Nano Letters 9 (2009) 1699–1703.
[14] Z. Gu, L. Zou, Z. Fang, W. Zhu, X. Zhong, Nanotechnology 19 (2008) 135604–135611.
[15] D.C. Pan, Q. Wang, S.C. Jiang, X.L. Ji, L.J. An, Advanced Materials 17 (2005) 176.
[16] D. Magde, R. Wong, P.G. Seybold, Photochemistry and Photobiology 75 (2002) 327–334.
[17] M. Kus, Ö. Haklı, C. Zafer, C. Varlikli, S. Demic, S. Icli, Organic Electronics 9 (2008) 757–766.
[18] A.L. Holt, J.M. Leger, S.A. Carter, Journal of Chemical Physics 123 (2005) 044704.
[19] J.R. Lakowicz, Principles of Fluorescence Spectroscopy Part 8, Kluwer Academic/Plenum Publisher, New York, 1999.
[20] L.C. Duong, The Structural Analyze by X ray, Publishing House for Science and Technology, Hanoi, 1984.
[21] S. Rana, J. Philip, B. Raj, Materials Chemistry and Physics 124 (2010) 264–269.
[22] R. Lee, H. Lai, European Polymer Journal 143 (2007) 715.
[23] D.Y. Kondakov, W.C. Lenhart, W.F. Nichols, Journal of Applied Physics 101 (2007) 024512.
[24] F. So, D. Kondakov, Advanced Materials 22 (2010) 3762–3777.
[25] T.P. Nguyen, Surface & Coatings Technology 206 (2011) 742–752.